Tandem phosphorylation within an intrinsically disordered region regulates ACTN4 function

Timothy Travers[1], **Hanshuang Shao**[2], **Brian A. Joughin**[3], **Douglas A. Lauffenburger**[4], **Alan Wells**[2], and **Carlos J. Camacho**[1,*]

[1]Department of Computational and Systems Biology, University of Pittsburgh, Pittsburgh, PA 15260, USA

[2]Department of Pathology, University of Pittsburgh, Pittsburgh, PA 15260, USA

[3]Koch Institute for Integrative Cancer Research, MIT Cambridge, MA 02139, USA

[4]Department of Biological Engineering, MIT, Cambridge, MA 02139, USA

Abstract

Phosphorylated residues occur preferentially in the intrinsically disordered regions of eukaryotic proteins. In the disordered N-terminal region of human α-actinin-4 (ACTN4), Tyr^4 and Tyr^{31} are phosphorylated in cells stimulated with epidermal growth factor (EGF), and a mutant with phosphorylation-mimicking mutations of both tyrosines exhibits reduced interaction with actin in vitro. Cleavage of ACTN4 by m-calpain, a protease that in motile cells is predominantly activated at the rear, removes the Tyr^4 site. Here, we found that introducing a phosphomimetic mutation at only Tyr^{31} was sufficient to inhibit the interaction with actin in vitro. However, molecular dynamics simulations predicted that Tyr^{31} is mostly buried and that phosphorylation of Tyr^4 would increase the solvent exposure and thus kinase accessibility of Tyr^{31}. In fibroblast cells, EGF stimulation increased tyrosine phosphorylation of a mutant form of ACTN4 with a phosphorylation-mimicking residue at Tyr^4, whereas a truncation mutant representing the product of m-calpain cleavage exhibited EGF-stimulated tyrosine phosphorylation at the background amount similar to that observed for a double phosphomimetic mutant of Tyr^4 and Tyr^{31}. We also found that inhibition of the receptor tyrosine kinases of the TAM family, such as AXL, blocked EGF-stimulated tyrosine phosphorylation of ACTN4. Mathematical modeling predicted that the kinetics of phosphorylation at Tyr^{31} can be dictated by the kinase affinity for Tyr^4. This study suggests that tandem-site phosphorylation within intrinsically disordered regions provides a mechanism for a site to function as a switch to reveal a nearby function-regulating site.

INTRODUCTION

Phosphorylation is an important and reversible mechanism for the regulation of protein function (1). In eukaryotic proteins, phosphorylation sites are found with higher frequency in intrinsically disordered regions (IDRs) than in structured regions (2), and frequently there are multiple phosphorylation sites within an IDR (3). Because signaling proteins have a higher proportion of residues in disordered regions than in other proteins (4–6), an understanding of how multiple phosphorylation events within IDRs regulate protein function is critical for generating a complete picture of cellular signaling. Here, we report evidence of a pair of functionally coupled phosphorylation sites within an IDR: One conserved phosphorylation site that modulated protein function was regulated by a "tandem" phosphorylation site that controlled the accessibility of the former site to its modifying kinase in a switch-like fashion.

The α-actinins (ACTNs) are a highly conserved family of actin-crosslinking proteins that play important roles during cellular remodeling of the cytoskeleton (7). The multiple spectrin repeats in ACTNs form antiparallel homodimers that crosslink actin filaments (8, 9). Among the four vertebrate ACTN isoforms, ACTN1 and ACTN4 are present ubiquitously in non-muscle cells; whereas ACTN2 and ACTN3 are restricted to myocyte lineages (10). In addition to filament crosslinking, ACTNs may bridge the cytoskeletal network to the cell membrane with ACTN4 in particular playing a critical role in cell motility (11–15).

Epidermal growth factor (EGF) stimulates cell migration. Two tyrosines, (Tyr^4 and Tyr^{31}) in the disordered N-terminal region of ACTN4 are the main sites phosphorylated in EGF-stimulated cells (16). In addition, a weaker phosphorylation signal that might include phosphorylated Tyr^{265} in the structured actin-binding domain (ABD) is also detected in these cells. Motile cells have defined front and rear (trailing) sides with distinct cytoskeletal dynamics (17, 18). The protease m-calpain (also known as CAPN2), for example, is predominantly activated at the rear of motile cells (19, 20). We have previously shown that m-calpain cleaves the ACTN4 N-terminal region such that the first 13 residues, including the Tyr^4 phosphorylation site, are removed (21).

Tyrosine phosphorylation within the disordered N-terminal region of the non-muscle ACTN isoforms regulates their actin binding activity in vitro (16, 22). Phosphorylation-mimicking mutations of ACTN4 at both Tyr^4 and Tyr^{31} show decreased actin binding (16). Similarly, phosphorylation of ACTN1 by focal adhesion kinase (FAK) at Tyr^{12}, which is homologous to Tyr^{31} in ACTN4, also decreases actin binding (22). Previously, we suggested that phosphorylation of ACTN4 Tyr^{31} results in a conformational change that latches the two calponin homology (CH) domains of the ABD into a closed conformation, thereby inhibiting the binding to actin filaments (23). The role of the phosphorylation site at Tyr^4 in the unstructured N-terminal region of ACTN4 is unknown.

To investigate further the functions of the two phosphorylated tyrosines in the N-terminal region of ACTN4, we performed in vitro actin-binding assays, molecular dynamics simulations (MDS), and phosphorylation assays in EGF-stimulated cells expressing (i) wild-

type ACTN4, (ii) phosphorylation-mimicking mutants at Tyr[4], Tyr[31], or both, or (iii) a truncation mutant representing the product of m-calpain cleavage within the N-terminal region. These studies indicated that only phosphorylated Tyr[31] was required to inhibit actin binding in vitro, and that Tyr[4] functioned as a switch site the phosphorylation of which was necessary to enable the phosphorylation of Tyr[31]. To determine the kinases that may be involved in phosphorylating these residues, we inspected the sequences for potential consensus motifs and performed experiments with pharmacological inhibitors of kinases that are predicted to phosphorylate those motifs. These experiments suggested that EGF-stimulated phosphorylation of ACTN4 involved the TAM family of receptor tyrosine kinases, such as AXL, a hypothesis we confirmed in cells.

Using mathematical modeling, we also showed that, for tandem phosphorylation sites within an IDR, fine-tuning of the kinase affinity to the switch site (for example, Tyr[4]) or the relative amounts of the kinase and phosphatase targeting that site would be sufficient to regulate the phosphorylation kinetics of the functional site (for example, Tyr[31] that functions as an inhibitor of actin binding). Thus, tandem phosphorylation sites within IDRs may enable the evolution of functional diversity.

RESULTS

Human ACTN4 Tyr[31] is a conserved phosphorylation site

To gain insight into the role of dual phosphorylation of the ACTN4 N-terminal region, we constructed a multiple sequence alignment of ACTNs from various species (Fig. 1A). In human ACTN1, phosphorylation of Tyr[12] is sufficient to reduce binding to actin filaments (22). The alignment showed that Tyr[31] of human ACTN4 represented the homologous residue to ACTN1 Tyr[12], suggesting that the phosphorylation of Tyr[31] is responsible for the observed inhibition in actin binding of ACTN4 upon EGF-induced dual phosphorylation of its N-terminal region (16). The alignment also showed that this tyrosine is conserved in all ACTN proteins analyzed, which indicates that a similar mechanism for regulating actin binding may exist for ACTNs in general. We note that in most of the ACTNs there are other tyrosines upstream of the conserved Tyr[31], however, only phosphorylation at ACTN4 Tyr[4] has so far been detected in this region (16). The region between the two phosphorylation sites in ACTN4 is uniquely characterized by the presence of a hydrophobic linker, whereas ACTN1 has a shorter hydrophilic stretch of residues next to Tyr[12]. The differences in the biochemical properties of the intervening amino acids suggests that the ACTN4 N-terminal region might adopt a more structurally-compact state than the ACTN1 N-terminal region (24, 25).

Phosphorylation-mimicking mutation of human ACTN4 Tyr[31] inhibits actin binding

We examined the importance of Tyr[31] in regulating the interaction of human ACTN4 with actin, using in vitro actin-binding assays with full-length ACTN4 constructs containing the phosphorylation-mimicking mutation of glutamic acid at Tyr[4], Tyr[31], or both (Fig. 1B). We found that the Y31E single mutant had a similar decrease in binding as the Y4/31E double mutant, whereas the Y4E single mutant exhibited binding similar to that of the wild-type ACTN4 (Fig. 1C). These results indicated that of the two N-terminal tyrosines that are

phosphorylated in response to EGF, phosphorylation of Tyr^{31} is likely functionally important for inhibiting the actin binding of ACTN4, similar to the role played by phosphorylated Tyr^{12} in ACTN1. Therefore, we refer to Tyr^{31} as the "function-regulating site."

Molecular dynamics simulations predict that phosphorylation of human ACTN4 Tyr⁴ is required for Tyr³¹ phosphorylation

To explore the role of Tyr^4 phosphorylation, we performed molecular dynamics simulations (MDS) of residues 1 to 57 (with residues 1 to 45 and residues 46 to 57 comprising the N-terminal region and the first helix of the CH1 domain, respectively) for both wild-type ACTN4 and the Y4E phosphomimetic mutant and assessed the solvent-accessible surface areas surrounding Tyr^4 and Tyr^{31}. Three independent simulations for the wild-type sequence predicted that the Tyr^4 side chain would be solvent exposed and that the Tyr^{31} side chain would be mostly buried (Fig. 2A) within a molten globule packed by two semistable antiparallel helices around Tyr^4 and Tyr^{31}. These simulations thus predicted that Tyr^4, but not Tyr^{31}, would be accessible for phosphorylation in the unphosphorylated protein. Simulations for the Y4E phosphomimetic predicted that the additional negative charge exposes the Tyr^{31} side chain to solvent (Fig. 2B) by swapping the molten globule to a mostly parallel helical arrangement. These models suggested that prior phosphorylation of Tyr^4 is needed for the function-regulating Tyr^{31} to become accessible to its kinase. Therefore, we refer to Tyr^4 as the "switch site."

ACTN4 contains an m-calpain cleavage site between residues Tyr^{13} and Gly^{14} in the N-terminal region (21), and cleavage at this site removes the Tyr^4 phosphorylation site. Simulations of the truncated N-terminal region predicted that Tyr^{31} would remain buried and inaccessible to its kinase (Fig. 2C), because the Tyr^{31} hydroxyl group was often observed to be engaged by a helical region between Pro^{15} and Ala^{22} that takes the place of the helix around Tyr^4 in the full protein.

Whereas tandem phosphorylation of ACTN4 is necessary to regulate its actin binding, phosphorylation of Tyr^{12} alone inhibits actin binding of ACTN1 (22). We also ran simulations of the hydrophilic N-terminal region of ACTN1 and, as expected, the Tyr^{12} side chain was predicted to be mostly exposed and kinase-accessible (Fig. 2D); the entire ACTN1 N-terminal was predicted to adopt a more extended structure than that predicted for the ACTN4 N-terminal.

Phosphorylation of Tyr³¹ depends on Tyr⁴ in human ACTN4

To test the prediction that Tyr^4 and its phosphorylation was required for Tyr^{31} phosphorylation, we expressed wild-type ACTN4 tagged with green fluorescent protein (GFP), a GFP-tagged Y4E mutant, and a GFP-tagged truncation mutant lacking the first 13 residues (14-911, representing the protein that would result from m-calpain cleavage) in NR6WT fibroblasts. We then tested for EGF-stimulated phosphorylation with an antibody that recognizes phosphotyrosine after immunoprecipitating the proteins with an antibody recognizing GFP (Fig. 3A). We found a strong signal likely representing phosphorylation of both Tyr^4 and Tyr^{31} in cells expressing wild-type ACTN4, whereas we detected less

phosphorylation, likely representing phosphorylation of mostly Tyr^{31}, in cells expressing the Y4E mutant (Fig. 3B). Assuming that the phosphotyrosine antibody recognizes these two sites equally, these results are consistent with previous observations that indicated Tyr^4 as the major site of phosphorylation upon EGF stimulation (16).

We also found that the truncated mutant had significantly reduced tyrosine phosphorylation compared to either the wild-type or Y4E constructs. These results indicated that Tyr^{31} phosphorylation occurred to a much lesser extent when Tyr^4 was not present and available for phosphorylation. Therefore, we proposed a mechanism by which an initially phosphorylated site reshapes the molten globule structure of an IDR and thereby enables kinase-accessibility of a nearby function-regulating phosphorylation site (Fig. 3C).

An aspartic acid adjacent to human ACTN4 Tyr^4 is important for phosphorylation

One approach to identifying kinases that may phosphorylate Tyr^4 and Tyr^{31} is to inspect the sequence surrounding those sites for conserved motifs recognized by specific kinases. We noted that the similarity of the sequence motif around human Tyr^4 and Tyr^{31}, MXD-**pY**-XA, suggested that a single class of kinases (or even the same kinase) may phosphorylate both sites. Hence, we postulated that mutations to either Asp^3 or Asp^{30} would lead to weaker kinase affinity for the adjacent Tyr^4 or Tyr^{31}, respectively, and decrease overall phosphorylation levels relative to that of the wild-type protein. MDS of N-terminal constructs containing either D3A or D30A mutations predicted that, contrary to the wild-type ACTN4 N-terminal region, Tyr^{31} phosphorylation would be decoupled from Tyr^4 phosphorylation, because Tyr^{31} was almost equally solvent exposed as in Y4E (Fig. 4A). Thus, considering the change in specificity of the binding site due to the aspartic acid mutations, we predicted that tyrosine phosphorylation of the D3A mutant in cells would be at least as much as that of the Y4E phosphomimetic mutant, because MDS predicted that both mutants had solvent-exposed Tyr^{31}. We also predicted that the D30A mutant would have at least as much tyrosine phosphorylation in cells as the Y31E phosphomimetic mutant, because the switch site (Tyr^4) would be exposed and have an unaltered phosphorylation consensus motif in both mutant versions of ACTN4.

To test these predictions, we expressed GFP-tagged constructs of human ACTN4 containing the single mutations D3A or D30A or the double mutation D3/30A in the fibroblast cell line and assayed for tyrosine phosphorylation of the GFP-tagged proteins immunoprecipitated from cells that were either exposed to EGF or not (Fig. 4B). In EGF-stimulated cells, the D3A mutant exhibited less phosphorylation than wild-type ACTN4 and more than Y4E (Fig. 4C), indicating that the mutation at Asp^3 decreased (but did not completely inhibit) Tyr^4 phosphorylation. EGF-stimulated D30A phosphorylation was not significantly different from that of wild-type ACTN4 and was higher than that of the Y31E mutant or D3/30A double mutant. These data indicated that the phosphorylation of ACTN4 Tyr^4 primarily depended on its surrounding sequence.

EGF-induced phosphorylation of ACTN4 is independent of FAK

FAK phosphorylates Tyr^{12} in the disordered N-terminal region of human ACTN1 (22). Because the kinase activity of FAK is inhibited in A431 epidermoid carcinoma cells upon

stimulation with EGF (26), we showed that EGF-induced phosphorylation of ACTN4 was unaffected by FAK inhibition (Figs. 5A and 5B). Moreover, consistent with the similarity between the sequence motif around human ACTN4 Tyr[31] (DY[31]MAQ) and ACTN1 Tyr[12] (DY[12]MQP), we found that EGF also stimulated tyrosine phosphorylation of GFP-tagged ACTN1 in a FAK-independent manner. This result suggested that there are at least two pathways by which the ACTN1 N-terminal region is phosphorylated: by FAK (in the absence of EGF) and by a FAK-independent pathway that is activated by EGF.

AXL may be involved in dual phosphorylation of the ACTN4 N-terminal region

We scanned for potential kinases of the ACTN4 Tyr[4] and Tyr[31] sites using PhosphoNET (http://www.phosphonet.ca) (27), which indicated that the most likely candidate for both sites is the receptor tyrosine kinase AXL. To check for the involvement of AXL, we analyzed the amount of tyrosine phosphorylation in GFP-tagged wild-type, Y4E, and Y31E ACTN4 constructs in cells that were exposed to EGF and also to various kinase inhibitors. As was shown previously (16), inhibition of the EGF receptor or the stress-activated kinase p38 blocked EGF-stimulated tyrosine phosphorylation for each of these constructs (Figs. 5C and 5D). We also found that R428, an inhibitor of the TAM (TYRO3, AXL, and MER) family of receptor tyrosine kinases (28), also reduced tyrosine phosphorylation for each of these constructs. Thus, EGF may stimulate a pathway that involves the kinase p38 and TAM family members, but does not involve FAK, to trigger the tyrosine phosphorylation of the ACTN4 N-terminal and thus inhibit the interaction of ACTN4 with actin.

Switch-like changes in Tyr[31] phosphorylation can arise by fine-tuning the kinase affinity for the Tyr[4] site

Integrating the signals arising from multiple phosphorylation and dephosphorylation events leads to complex nonlinear responses, which can be explored using mathematical modeling (29, 30). Previous findings from models of multisite sequential phosphorylation (31–33) do not apply to our tandem phosphorylation model for ACTN4, because here the actin-binding inhibited state only requires phosphorylation of one of the paired sites, Tyr[31]. Hence, to understand the constraints imposed by the switch site at Tyr[4] on the phosphorylation of the "function-regulating site" at Tyr[31], we used a mathematical modeling approach (see Methods) to compare the steady-state proportion of phosphorylation on the function-regulating site in a single-site model (for example, at the single Tyr[12] site in ACTN1) and in a two-site tandem model undergoing sequential phosphorylation (for example, in ACTN4). We solved these models assuming that a single kinase and a single phosphatase act on the phosphorylation sites and that the catalytic rates of the kinase and phosphatase are the same. Note that we follow here the notation of Rowland *et al.* (30), with the Michaelis constant for the kinase acting on Tyr[4] denoted as $K_{M,K}^{Y4}$ (and similar notation for the other constants).

For the single-site model (Fig. 6A), which is also referred to as the Goldbeter-Koshland loop (34), phosphorylation of the function-regulating site increased hyperbolically with the ratio of the activities (taken here to be proportional to the concentrations) of kinase to phosphatase at nonsaturating conditions of the substrate. However, at saturating concentrations the system shows an ultrasensitive switch-like behavior such that the amount of phosphorylated substrate abruptly shifts as the ratio of kinase to phosphatase activity

changes: Maximally-phosphorylated Tyr^{12} already occurs once the kinase activity becomes slightly greater than the phosphatase activity, and shifts to minimally-phosphorylated Tyr^{12} once phosphatase activity becomes slightly greater than kinase activity.

For the two-site tandem model, we found that when the relative affinity of the kinase for the switch site (Tyr^4 of ACTN4) was lowered by 50-fold compared to the affinity for the function-regulating site (Tyr^{31} in ACTN4), phosphorylation of the latter site was dramatically lower unless ACTN4 was present at saturating concentrations and there was around twice as much kinase activity to phosphatase activity (Fig. 6B). For unsaturated conditions, maximum phosphorylation resulted from a hyperbolic (instead of a switch-like) response only upon reaching a large enough kinase to phosphatase activity ratio. A similar type of behavior is for single-site systems in which the kinase and phosphatase can be treated as unsaturated and saturated, respectively (35). However, if the kinase is set to have similar affinities for both sites, the phosphorylation kinetics of the function-regulating site exhibited switch-like behavior similar to the single-site model for substrate concentrations ten times or more larger than the kinase Michaelis constant of the kinase for both sites (Fig. 6C, black curve; note that $K_{M,K}{}^{Y31}$ is equal to $K_{M,K}{}^{Y4}$ in this plot).

Moreover, our analysis revealed that as long as the kinase affinity towards the switch site is higher than its affinity towards the function-regulating site ($K_{M,K}{}^{Y4}$ $K_{M,K}{}^{Y31}$), a switch-like phosphorylation response with respect to the ratio of kinase to phosphatase activities is always observed (Fig. 6D). This is consistent with Tyr^4 and Tyr^{31} serving as major and minor sites of phosphorylation, respectively (16) (Figs. 4C and 5D). Note that quantitatively, the results in Fig. 6D are identical to that for a two-kinase, one-phosphatase model system in which the two kinases (denoted K1 and K2) would have the same concentration but varying affinities for their corresponding site (with $K_{M,K1}{}^{Y31}/K_{M,K2}{}^{Y4}$ in one of the axes in Fig. 6D). In this theoretical two-kinase, one-phosphatase model, a switch-like response would occur if $K_{M,K2}{}^{Y4} < K_{M,K1}{}^{Y31}$ and a low level response would occur if $K_{M,K2}{}^{Y4} > K_{M,K1}{}^{Y31}$. From an evolutionary point of view, we note that in order for the tandem phosphorylation site Tyr^4 to efficiently work as a toggle for Tyr^{31} phosphorylation, it is sufficient to evolve the appropriate kinase affinity to the Tyr^4 site ($K_{M,K}{}^{Y4}$), while leaving the parameters related to the Tyr^{31} site unchanged.

DISCUSSION

By functioning as molecular switches, posttranslational modifications can mediate diverse signaling pathways. Using insights from MDS and mathematical modeling, our findings provide a framework for understanding a previously uncharacterized molecular switch that facilitates context-dependent regulation. On the basis of sequence similarity with other ACTN isoforms and in vitro actin-binding results, we concluded that phosphorylation of Tyr^{31} inhibits actin binding, likely by latching both CH domains in a closed conformation (23). MDS predicted that in the N-terminal region of wild-type ACTN4, Tyr^4 and Tyr^{31} are mostly accessible and inaccessible, respectively, for phosphorylation and that Tyr^4 phosphorylation leads to structural changes in the IDR that exposes Tyr^{31} to make it kinase accessible. Thus, we proposed that the phosphorylation state of Tyr^4 acts as a switch that determines whether the function-regulating site Tyr^{31} can become phosphorylated.

By utilizing a second phosphorylation site 27 residues away from the function-regulating site in the intrinsically disordered N-terminal region of ACTN4, the cell may differentially regulate actin crosslinking through the locale-specific presence of m-calpain and locale-specific activation of the kinases that phosphorylate the tandem sites. Our modeling also indicated that by adding a switch site, optimizing the phosphorylation of a nearby functional site within an IDR can be achieved simply by fine-tuning the kinase affinity of the switch relative to that of the functional site. We note that developing a tandem phosphorylation mechanism within a structured protein region to control the solvent exposure of a function-regulating site would be more complicated, and, for example, entail evolving an entire phosphorylatable binding partner, either as another protein or as a separate domain in the same protein, which can reversibly bind and cover this site Thus, the evolution of tandem phosphorylation sites within IDRs poses advantages relative to their evolution within structured domains, which is also consistent with the higher mutation rates observed in IDRs (36).

Our results indicate that cytoplasmic FAK involvement is not necessary for EGF-induced tyrosine phosphorylation of ACTN4 and ACTN1. We instead found that AXL or other TAM family members may be involved in the EGF-stimulated tyrosine phosphorylation of ACTN4. Expression of both *AXL* and *ACTN4* is increased in cells from invasive endometrial tissue of patients with endometriosis (37), which may be a precursor of ovarian cancer (38). In addition, AXL can be transactivated by the EGF receptor (39). AXL has also been implicated in reorganization of the actin cytoskeleton and migration of neuronal cells, with activation of p38 occurring downstream of AXL (40, 41). Pending further investigation of the role of p38 in fibroblast cell migration, receptor tyrosine kinase-mediated phosphorylation of Tyr^4 and Tyr^{31} is consistent with the predominant localization of ACTN4 at the cytosolic side of the plasma membrane to participate in actin cytoskeleton remodeling (42, 43).

In addition to dual phosphorylation of Tyr^4 and Tyr^{31} in the disordered N-terminal region of ACTN4, EGF also stimulates a less easily detected phosphorylation of ACTN4 that may include phosphorylation of Tyr^{265}, which is located in the ABD (16). Therefore, we interpret the tyrosine phosphorylation detected in cells expressing the Y4E mutant as primarily resulting from phosphorylation of Tyr^{31} and that in cells expressing the Y31E mutant as representing phosphorylation of Tyr^4.

We propose that tandem phosphorylation of the ACTN4 N-terminal region provides a rationale for locale-specific adhesion contacts during cell motility mediated by m-calpain, which is activated only at the rear of motile cells (19, 20). Namely, at the same time that the leading edge of the cell protrudes and makes new adhesion contacts with the outside matrix, the rear of the cell has to remain stably attached to the matrix through its own adhesion contacts. Hence, by cleaving the ACTN4 N-terminal region such that Tyr^{31} is no longer accessible for phosphorylation, even in the presence of EGF at the rear end of motile cells (44), m-calpain would stabilize the crosslinks between ACTN4 and F-actin to the cell membrane at the cell rear (21). Subsequently, m-calpain cleavage of talin loosens linkages between the actin cytoskeleton and adhesion plaques (45) to enable the cell body to move forward with the cell membrane. At the leading edge where m-calpain is not present, EGF-

induced tandem phosphorylation of the ACTN4 N-terminal region reduces actin binding, enabling dynamic restructuring of the actin network so that the leading edge extends forward and forms new contacts. In our model, tandem phosphorylation of ACTN4 in conjunction with m-calpain leads to locale-specific ACTN4 function such that at the front end EGF induces reduction of actin binding, while at the rear m-calpain cleavage stabilizes the ACTN4-actin interaction. We note that the m-calpain cleavage site is not conserved in the other three vertebrate ACTN isoforms (Fig. 1). The conservation of both the cleavage and tandem phosphorylation sites only in vertebrate ACTN4 suggests that tandem phosphorylation in ACTN4 co-evolved with a mechanism by which the Tyr^4 switch can be permanently turned off, disabling the main regulatory pathway that inhibits actin binding by ACTN4.

We anticipate that many other systems could exhibit a similar tandem —switch site and function-regulating site— mechanism of regulation and that this type of regulation could involve multiple kinases. Other systems with similar designs have been described. For instance, structural analysis of two tyrosine phosphorylation sites that are separated by 34 residues in the cytoplasmic domain of LRP1 (low density lipoprotein receptor-related protein) showed that the Tyr^{4507} site in the membrane-distal NPXY motif is fully solvent-exposed, while the Tyr^{4473} site in the membrane-proximal NPXY motif is initially buried but has increased solvent exposure and kinase accessibility upon phosphorylation at Tyr^{4507} (46). Analogous to the roles of Tyr^{31} and Tyr^4 in ACTN4, Tyr^{4473} phosphorylation is the functional site that inhibits binding to Snx17 (sorting nexin 17), and phosphorylation of only the Tyr^{4507} switch did not impact this binding (46). Another system with potential tandem phosphorylation sites is the C-terminal region of STAT1 (signal transducer and activator of transcription 1) that has two phosphorylation sites, Tyr^{701} and Ser^{727}, which are separated by 26 residues and for which Ser^{727} phosphorylation depends on prior phosphorylation of Tyr^{701} in response to interferons (47). The observation that IDRs have a higher propensity for phosphorylation sites suggests that tandem phosphorylation within IDRs is another mechanism to regulate protein function.

MATERIALS AND METHODS

Multiple sequence alignment and phylogenetic tree construction

ACTN protein sequences from various species were obtained from the NCBI protein database. Multiple sequence alignment and phylogenetic tree construction for these sequences were done using the interface provided by the Phylogeny.fr web service (48). The alignment was constructed with MUSCLE (49), using default parameters provided by the web service. The maximum likelihood phylogenetic tree was then constructed from this alignment using PhyML (50), also using default parameters provided by the web service. Statistical support for the tree branches was computed by bootstrapping with 100 replicates. TreeDyn (51) was used for rendering the phylogenetic tree.

Molecular dynamics simulations

All MDS used explicit solvent and were performed with the GPU-accelerated pmemd.cuda program from Amber version 14 (52, 53) using the Amber ff14SB force field. The starting

conformation for the ACTN4 wild-type N-terminal region was taken from an earlier implicit-solvent MDS, which started from a fully-extended conformation of residues 1 to 45 and showed burying of Tyr[31] (23). This conformation was attached to a helical segment comprising residues 46 to 57 from the first helix of the structured CH1 domain. The C-terminus of this entire construct was neutralized using an N-methylamide (NME) patch. To get the starting conformations for the various ACTN4 mutant sequences, point mutations (Y4E, D3A, D30A) and truncations (removal of residues 1 to 13 to model m-calpain cleavage) were then done using PyMOL (54). Similarly, to get the starting conformation for the ACTN1 wild-type N-terminal region, point mutations and truncations were done such that the structure around the conserved tyrosine phosphorylation site (Tyr[31] or Tyr[12] in ACTN4 or ACTN1, respectively) remained intact. All systems were solvated with TIP3P water molecules (55) in an octahedral box, and counter ions were added to neutralize the system charge. A cutoff of 8.0 Å was used for calculating short-range Lennard-Jones and electrostatic interactions, and long-range electrostatic contributions were computed using the particle mesh Ewald approach (56). An AMBER implementation of the hydrogen mass repartitioning scheme (57) allowed a time step of 4 fs to be used. All bond lengths involving hydrogen were kept constant using SHAKE (or SETTLE for water) (58, 59). Initial energy minimization was performed using steepest descent for 1000 steps then conjugate gradient minimization for 1000 steps. This was followed by temperature equilibration at 300 K for 50 ps under canonical (conserved number of particles [N], volume [V], and temperature [T]; or NVT) ensemble conditions, and then pressure equilibration at 1 atm and 300 K for another 50 ps under isothermal-isobaric (conserved number of particles [N], pressure [P], and temperature [T]; or NPT) ensemble conditions. All heavy atoms had position restraints up to this point. This was followed by further equilibration for 100 ns and then a production run for 500 ns, all under NVT ensemble conditions at 300 K and with position restraints on only the backbone heavy atoms comprising the helical segment from CH1. All MDS were done with triplicate runs, for a total sampling time of 1.5 μs. VMD (60) was used for trajectory visualization and SASA computations. Moving averages at every nanosecond were computed and plotted for the relative SASA.

Rule-based mathematical modeling simulations

Reaction rules to describe the single-site model and the 1-kinase/1-phosphatase (1K1P) two-site tandem model were implemented using BioNetGen v2.2.5 (61), which generates a complete set of ordinary differential equations (ODEs) for these models. The ODEs were then numerically integrated using the CVODE interface provided by BioNetGen until steady-state levels were reached. Details on the reaction rules and parameter values used for these models are provided in the Supplementary Notes.

ACTN4 constructs and experimental assays

Expression of wild-type ACTN4 and ACTN1 and various mutant ACTN4 constructs (Y4E, Y31E, Y4/31E, D3A, D30A, D3/30A, and truncation mutant 14-911), F-actin sedimentation

---

assays, and phosphorylation assays were all performed as described previously (16, 21). In brief, all ACTN4 mutagenesis was performed using PCR followed by DNA sequencing analysis to confirm mutations. Wild-type and mutant ACTN4, and wild-type ACTN1, constructs were then cloned into vector pET-28a for expression in bacterial cells and pEGFP-N1 for expression in mammalian cells. For actin-binding assays, 10 μg ACTN4 that was purified from bacteria was incubated with 20 μg actin (Sigma) in actin-binding buffer (10 mM Tris-HCl pH 7.4, 2mM $MgCl_2$, 120 mM NaCl, 0.5 mM ATP, and 0.5 mM EDTA) at room temperature for 1 hour followed by centrifugation at 100,000g for 40 minutes. Supernatant was collected and the pellet was briefly and carefully rinsed with water and dissolved in 2× Laemmli sample buffer. After boiling for 4 minutes, proteins were run on SDS-PAGE followed by Coomassie staining.

For phosphorylation assays, NR6WT fibroblast cells that had been transiently transfected with ACTN4 or ACTN1 plasmids using Lipofectamine 2000 (Life Technologies, catalog # 11668019) according to the manufacturer's instructions were starved with quiescence medium (α-MEM [catalog no. 15-012-CV; Cellgro, Lawrence KS] with 0.1% dialyzed fetal bovine serum, 1× nonessential amino acids, 1× sodium pyruvate, 1× streptomycin/penicillin, and 2 mM L-glutamine) for 18 hours and then pretreated with appropriate inhibitors [10 μM FAK inhibitor II (EMD Millipore, Calbiochem, catalog # 324878); 10 μM EGFR inhibitor PD153035 (EMD Millipore, Calbiochem, catalog # 234490-1MG); 15 μM p38 inhibitor SB203580 (EMD Milllipore, Calbiochem, catalog # 19-135); or 15 μM TAM inhibitor R428 (ApexBio, catalog # A8329)] for 30 minutes prior to treatment with 10 nM EGF for 1 hour. Cells were then harvested and lysed, and GFP-tagged protein was immunoprecipitated with monoclonal GFP antibody (Life Technology, Catalog # A-11120) followed by SDS-PAGE and immunoblotting against phosphorylated Tyr (Cell signaling Technology, catalog # 9411). After immunoblotting, the PVDF membrane was stripped of antibodies and stained with Coomassie blue G-250 to detect the amount of ACTN4-eGFP protein. This approach was further validated by immunodetection of ACTN4 or the GFP tag. Quantitative analysis was performed using ImageJ software (62).

Statistical analysis

Plotted experimental data are shown as mean values ± SEM. Two-sided Student's t test was used for comparison of sample means. P < 0.05 was considered to be statistically significant. All statistical analysis were performed in Microsoft Excel version 2013.

Acknowledgments

REFERENCES AND NOTES

1. Cohen P. The regulation of protein function by multisite phosphorylation--a 25 year update. Trends Biochem. Sci. 2000; 25:596–601. [PubMed: 11116185]

2. Iakoucheva LM, Radivojac P, Brown CJ, O'Connor TR, Sikes JG, Obradovic Z, Dunker AK. The importance of intrinsic disorder for protein phosphorylation. Nucleic Acids Res. 2004; 32:1037–1049. [PubMed: 14960716]

3. Tyanova S, Cox J, Olsen J, Mann M, Frishman D. Phosphorylation variation during the cell cycle scales with structural propensities of proteins. PLoS Comput. Biol. 2013; 9:e1002842. [PubMed: 23326221]

4. Liu J, Faeder JR, Camacho CJ. Toward a quantitative theory of intrinsically disordered proteins and their function. Proc. Natl. Acad. Sci. 2009; 106:19819–19823. [PubMed: 19903882]

5. Dyson HJ, Wright PE. Intrinsically unstructured proteins and their functions. Nat. Rev. Mol. Cell Biol. 2005; 6:197–208. [PubMed: 15738986]

6. Iakoucheva LM, Brown CJ, Lawson JD, Obradovic Z, Dunker AK. Intrinsic disorder in cell-signaling and cancer-associated proteins. J. Mol. Biol. 2002; 323:573–584. [PubMed: 12381310]

7. Otey CA, Carpen O. Alpha-actinin revisited: a fresh look at an old player. Cell. Motil. Cytoskeleton. 2004; 58:104–111. [PubMed: 15083532]

8. Flood G, Kahana E, Gilmore AP, Rowe AJ, Gratzer WB, Critchley DR. Association of structural repeats in the α-actinin rod domain. Alignment of inter-subunit interactions. J. Mol. Biol. 1995; 252:227–234. [PubMed: 7674303]

9. Flood G, Rowe AJ, Critchley DR, Gratzer WB. Further analysis of the role of spectrin repeat motifs in α-actinin dimer formation. Eur. Biophys. J. 1997; 25:431–435. [PubMed: 9188165]

10. Sjöblom B, Salmazo A, Djinovi -Carugo K. Alpha-actinin structure and regulation. Cell Mol. Life Sci. 2008; 65:2688–2701. [PubMed: 18488141]

11. Shao H, Wang JH-C, Pollak MR, Wells A. α-Actinin-4 is essential for maintaining the spreading, motility and contractility of fibroblasts. PLoS One. 2010; 5:e13921. [PubMed: 21085685]

12. Fraley TS, Pereira CB, Tran TC, Singleton C, Greenwood JA. Phosphoinositide binding regulates alpha-actinin dynamics: mechanism for modulating cytoskeletal remodeling. J. Biol. Chem. 2005; 280:15479–15482. [PubMed: 15710624]

13. Dandapani SV, Sugimoto H, Matthews BD, Kolb RJ, Sinha S, Gerszten RE, Zhou J, Ingber DE, Kalluri R, Pollak MR. α-Actinin-4 is required for normal podocyte adhesion. J. Biol. Chem. 2007; 282:467–477. [PubMed: 17082197]

14. Kanchanawong P, Shtengel G, Pasapera AM, Ramko EB, Davidson MW, Hess HF, Waterman CM. Nanoscale architecture of integrin-based cell adhesions. Nature. 2010; 468:580–584. [PubMed: 21107430]

15. Rosa-Cusachs P, del Rio A, Puklin-Faucher E, Gauthier NC, Biais N, Sheetz MP. Integrin-dependent force transmission to the extracellular matrix by α-actinin triggers adhesion maturation. Proc. Natl. Acad. Sci. 2013; 110:E1361–E1370. [PubMed: 23515331]

16. Shao H, Wu C, Wells A. Phosphorylation of α-actinin-4 upon epidermal growth factor exposure regulates its interaction with actin. J. Biol. Chem. 2010; 285:2591–2600. [PubMed: 19920151]

17. Lauffenburger DA, Horwitz AF. Cell migration: a physically integrated molecular process. Cell. 1996; 84:359–369. [PubMed: 8608589]

18. Chou J, Stolz DB, Burke NA, Watkins SC, Wells A. Distribution of gelsolin and phosphoinositol 4,5-biphosphate in lamellipodia during EGF-induced motility. Int. J. Biochem. Cell Biol. 2002; 34:776–790. [PubMed: 11950594]

19. Shao H, Chou J, Baty CJ, Burke NA, Watkins SC, Stolz DB, Wells A. Spatial localization of m-calpain to the plasma membrane by phosphoinositide biphosphate binding during epidermal growth factor receptor-mediated activation. Mol. Cell Biol. 2006; 26:5481–5496. [PubMed: 16809781]

20. Leloup L, Shao H, Bae YH, Deasy B, Stolz D, Roy P, Wells A. m-Calpain activation is regulated by its membrane localization and by its binding to phosphatidylinositol 4,5-bisphosphate. J. Biol. Chem. 2010; 285:33549–33566. [PubMed: 20729206]

21. Shao H, Travers T, Camacho CJ, Wells A. The carboxyl tail of alpha-actinin-4 regulates its susceptibility to m-calpain and thus functions in cell migration and spreading. Int. J. Biochem. Cell Biol. 2013; 45:1051–1063. [PubMed: 23466492]

22. Izaguirre G, Aguirre L, Hu Y-P, Lee HY, Schlaepfer DD, Aneskievich BJ, Haimovich B. The cytoskeletal/non-muscle isoform of α-actinin is phosphorylated on its actin-binding domain by the focal adhesion kinase. J. Biol. Chem. 2001; 276:28676–28685. [PubMed: 11369769]

23. Travers T, Shao H, Wells A, Camacho CJ. Modeling the assembly of the multiple domains of α-actinin-4 and its role in actin cross-linking. Biophys. J. 2013; 104:705–715. [PubMed: 23442921]

24. Uversky VN, Santambrogio C, Brocca S, Grandori R. Length-dependent compaction of intrinsically disordered proteins. FEBS Lett. 2012; 586:70–73. [PubMed: 22138473]

25. Das RK, Pappu RV. Conformations of intrinsically disordered proteins are influenced by linear sequence distributions of oppositely charged residues. Proc. Natl. Acad. Sci. 2013; 110:13392–13397. [PubMed: 23901099]

26. Lu Z, Jiang G, Blume-Jensen P, Hunter T. Epidermal growth factor-induced tumor cell invasion and metastasis initiated by dephosphorylation and downregulation of focal adhesion kinase. Mol. Cell Biol. 2001; 21:4016–4031. [PubMed: 11359909]

27. Safaei J, Ma uch J, Gupta A, Stacho L, Pelech S. Prediction of 492 human protein kinase substrate specificities. Proteome Sci. 9(Suppl 1):S6. [PubMed: 22165948]

28. Holland SJ, Pan A, Franci C, Hu Y, Chang B, Li W, Duan M, Torneros A, Yu J, Heckrodt TJ, Zhang J, Ding P, Apatira A, Chua J, Brandt R, Pine P, Goff D, Singh R, Payan DG, Hitoshi Y. R428, a selective small molecule inhibitor of Axl kinase, blocks tumor spread and prolongs survival in models of metastatic breast cancer. Cancer Res. 2010; 70:1544–1554. [PubMed: 20145120]

29. Gough NR, Foley JF. Focus issue: systems analysis of protein Phosphorylation. Sci. Signal. 2010; 3:eg6. [PubMed: 20807952]

30. Rowland MA, Fontana W, Deeds EJ. Crosstalk and competition in signaling networks. Biophys. J. 2012; 103:2389–2398. [PubMed: 23283238]

31. Salazar C, Höfer T. Versatile regulation of multisite protein phosphorylation by the order of phosphate processing and protein-protein interactions. FEBS J. 2007; 274:1046–1061. [PubMed: 17257173]

32. Gunawardena J. Multisite protein phosphorylation makes a good threshold but can be a poor switch. Proc. Natl. Acad. Sci. 2005; 102:14617–14622. [PubMed: 16195377]

33. Wang L, Nie Q, Enciso G. Nonessential sites improve phosphorylation switch. Biophys. J. 2010; 99:L41–L43. [PubMed: 20858409]

34. Goldbeter A, Koshland DE Jr. An amplified sensitivity arising from covalent modification in biological systems. Proc. Natl. Acad. Sci. 1981; 78:6840–6844. [PubMed: 6947258]

35. Gomez-Uribe C, Verghese GC, Mirny LA. Operating regimes of signaling cycles: statics, dynamics, and noise filtering. PLoS Comput. Biol. 2007; 3:e246. [PubMed: 18159939]

36. Brown CJ, Johnson AK, Daughdrill GW. Comparing models of evolution for ordered and disodered proteins. Mol. Biol. Evol. 2010; 27:609–621. [PubMed: 19923193]

37. Honda H, Barrueto FF, Gogusev J, Im DD, Morin PJ. Serial analysis of gene expression reveals differential expression between endometriosis and normal endometrium. Possible roles for AXL and SHC1 in the pathogenesis of endometriosis. Reprod. Biol. Endocrinol. 2008; 6:59. [PubMed: 19055724]

38. Prowse AH, Manek S, Varma R, Liu J, Godwin AK, Maher ER, Tomlinson IPM, Kennedy SH. Molecular genetic evidence that endometriosis is a precursor of ovarian cancer. Int. J. Cancer. 2006; 119:556–562. [PubMed: 16506222]

39. Meyer AS, Miller MA, Gertler FB, Lauffenburger DA. The receptor AXL diversifies EGFR signaling and limits the response to EGFR-targeted inhibitors in triple-negative breast cancer cells. Sci. Signal. 2013; 6:ra66. [PubMed: 23921085]

40. Allen MP, Linseman DA, Udo H, Xu M, Schaack JB, Varnum B, Kandel ER, Heidenreich KA, Wierman ME. Novel mechanism for gonadotropin-releasing hormone neuronal migration involving Gas6/Ark signaling to p38 mitogen-activated protein kinase. Mol. Cell Biol. 2002; 22:599–613. [PubMed: 11756555]

41. Nielsen-Preiss SM, Allen MP, Xu M, Linseman DA, Pawlowski JE, Bouchard RJ, Varnum BC, Heidenreich KA, Wierman ME. Adhesion-related kinase induction of migration requires phosphatidylinositol-3-kinase and Ras stimulation of Rac activity in immortalized gonadotropin-releasing hormone neuronal cells. Endocrinology. 2007; 148:2806–2814. [PubMed: 17332061]

42. Gonzalez AM, Otey C, Edlund M, Jones JCR. Interactions of a hemidesmosome component and actinin family members. J. Cell Sci. 2001; 114:4197–4206. [PubMed: 11739652]

43. Michaud JL, Chaisson KM, Parks RJ, Kennedy CR. FSGS-associated alpha-actinin-4 (K256E) impairs cytoskeletal dynamics in podocytes. Kidney Int. 2006; 70:1054–1061. [PubMed: 16837921]

44. Bailly M, Wyckoff J, Bouzahzah B, Hammerman R, Sylvestre V, Cammer M, Pestell R, Segall JE. Epidermal growth factor distribution during chemotactic responses. Mol. Biol. Cell. 2000; 11:3873–3883. [PubMed: 11071913]

45. Franco SJ, Rodgers MA, Perrin BJ, Han J, Bennin DA, Critchley DR, Huttenlocher A. Calpain-mediated proteolysis of talin regulates adhesion dynamics. Nat. Cell Biol. 2004; 6:977–983. [PubMed: 15448700]

46. Betts GN, van der Geer P, Komives EA. Structural and functional consequences of tyrosine phosphorylation in the LRP1 cytoplasmic domain. J. Biol. Chem. 2008; 283:15656–15664. [PubMed: 18381291]

47. Sadzak I, Schiff M, Gattermeier I, Glinitzer R, Sauer I, Saalmüller A, Yang E, Schaljo B, Kovarik P. Recruitment of Stat1 to chromatin is required for interferon-induced serine phosphorylation of Stat1 transactivation domain. Proc. Natl. Acad. Sci. 2008; 105:8944–8949. [PubMed: 18574148]

48. Dereeper A, Guignon V, Blanc G, Audic S, Buffet S, Chevenet F, Dufayard J-F, Guindon S, Lefort V, Lescot M, Claverie J-M, Gascuel O. Phylogeny.fr: robust phylogenetic analysis for the non-specialist. Nucleic Acids Res. 2008; 36:W465–W469. [PubMed: 18424797]

49. Edgar RC. MUSCLE: multiple sequence alignment with high accuracy and high throughput. Nucleic Acids Res. 2004; 32:1792–1797. [PubMed: 15034147]

50. Guindon S, Dufayard J-F, Lefort V, Anisimova M, Hordijk W, Gascuel O. New algorithms and methods to estimate maximum-likelihood phylogenies: assessing the performance of PhyML 3.0. Syst. Biol. 2010; 59:307–321. [PubMed: 20525638]

51. Chevenet F, Brun C, Bañuls AL, Jacq B, Christen R. TreeDyn: towards dynamic graphics and annotations for analyses of trees. BMC Bioinformatics. 2006; 7:439. [PubMed: 17032440]

52. Case, DA.; Babin, V.; Berryman, JT.; Betz, RM.; Cai, Q.; Cerutti, DS.; Cheatham, TE., III; Darden, TA.; Duke, RE.; Gohlke, H.; Goetz, AW.; Gusarov, S.; Homeyer, N.; Janowski, P.; Kaus, J.; Kolossváry, I.; Kovalenko, A.; Lee, TS.; LeGrand, S.; Luchko, T.; Luo, R.; Madej, B.; Merz, KM.; Paesani, F.; Roe, DR.; Roitberg, A.; Sagui, C.; Salomon-Ferrer, R.; Seabra, G.; Simmerling, CL.; Smith, W.; Swails, J.; Walker, RC.; Wang, J.; Wolf, RM.; Wu, X.; Kollman, PA. AMBER 14. San Francisco: University of California; 2014.

53. Salomon-Ferrer R, Goetz AW, Poole D, LeGrand S, Walker RC. Routine microsecond molecular dynamics simulations with AMBER on GPUs. 2. Explicit solvent particle mesh Ewald. J. Chem. Theory Comput. 2013; 9:3878–3888.

54. The PyMOL Molecular Graphics System, Version 1.7.4. LLC: Schrödinger; 2015.

55. Jorgensen WL. Quantum and statistical mechanical studies of liquids. 10. Transferable intermolecular potential functions for water, alcohols, and ethers. Application to liquid water. J. Am. Chem. Soc. 1981; 103:335–340.

56. Darden T, York D, Pedersen L. Particle mesh Ewald: An N·log(N) method for Ewald sums in large systems. J. Chem. Phys. 1993; 98:10089–10092.

57. Feenstra KA, Hess B, Berendsen HJC. Improving efficiency of large time-scale molecular dynamics simulations of hydrogen-rich systems. J. Comput. Chem. 1999; 20:786–798.

58. Ryckaert J-P, Ciccotti G, Berendsen HJC. Numerical integration of the cartesian equations of motion of a system with constraints: molecular dynamics of n-alkanes. J. Comput. Phys. 1977; 23:327–341.

59. Miyamoto S, Kollman PA. SETTLE: an analytical version of the SHAKE and RATTLE algorithm for rigid water models. J. Comput. Chem. 1992; 13:952–962.

60. Humphrey W, Dalke A, Schulten K. VMD: visual molecular dynamics. J. Mol. Graph. 1996; 14:33–38. 27–28. [PubMed: 8744570]

61. Hlavacek WS, Faeder JR, Blinov ML, Posner RG, Hucka M, Fontana W. Rules for modeling signal-transduction systems. Sci. STKE. 2006; 2006:re6. [PubMed: 16849649]

62. Schneider CA, Rasband WS, Eliceiri KW. NIH Image to ImageJ: 25 years of image analysis. Nat. Methods. 2012; 9:671–675. [PubMed: 22930834]
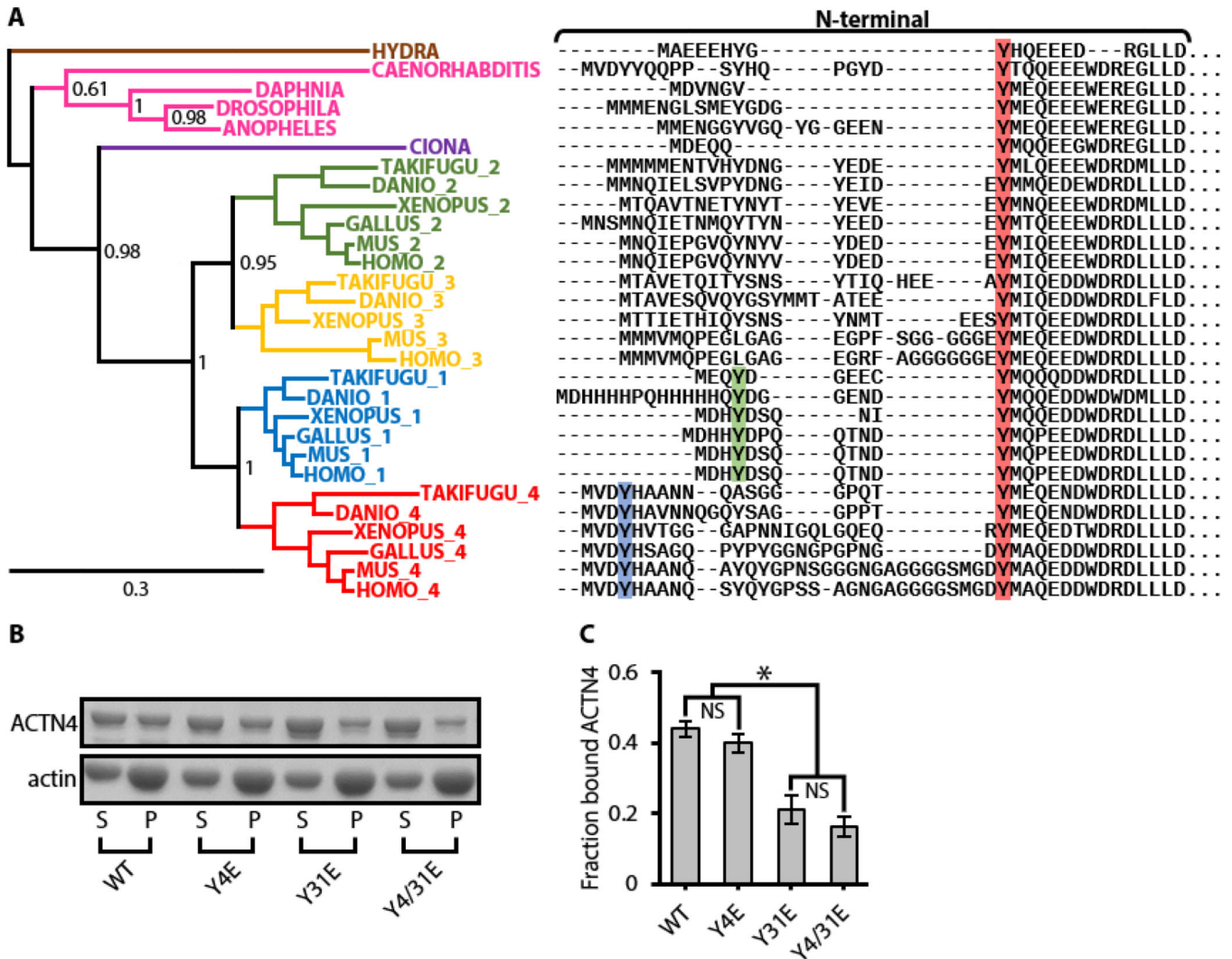
Figure 1. Phosphorylation of Tyr[31] in ACTN4 is necessary and sufficient to inhibit actin binding
(**A**) Multiple sequence alignment (right) and phylogenetic tree (left) of ACTN isoforms from various animal species. Only the disordered N-terminal regions are shown in the alignment. The column colored in red contains the highly conserved Tyr[31] from human ACTN4 (HOMO_4), which is homologous to Tyr[12] in human ACTN1 (HOMO_1). Columns containing the Tyr[4] sites of ACTN4 and ACTN1 are colored in blue and green, respectively. Note that the ACTN4 sequences are characterized by the insertion of a hydrophobic linker between Tyr[4] and Tyr[31]. Numbers to the right of branch points in the phylogenetic tree represent bootstrap support based on 100 replicates. Branches within the ACTN1-4 clusters all have bootstrap support values of at least 0.98. Scale bar represents the number of substitutions per site. (**B**) Representative gel of actin-binding assay for WT, Y4E, Y31E, and Y4/31E constructs of ACTN4, following ultracentrifugation and separation of supernatant (S) and pellet (P). (**C**) Quantitation of three actin-binding experiments for the fraction of bound ACTN4 in the pellet. Error bars indicate SEM. [* $P < 0.05$ based on two-sided Student's t-test. NS, not significant.] The asterisk applies to the following four pairwise comparisons: WT vs. Y31E, WT vs. Y4/31E, Y4E vs. Y31E, and Y4E vs. Y4/31E.
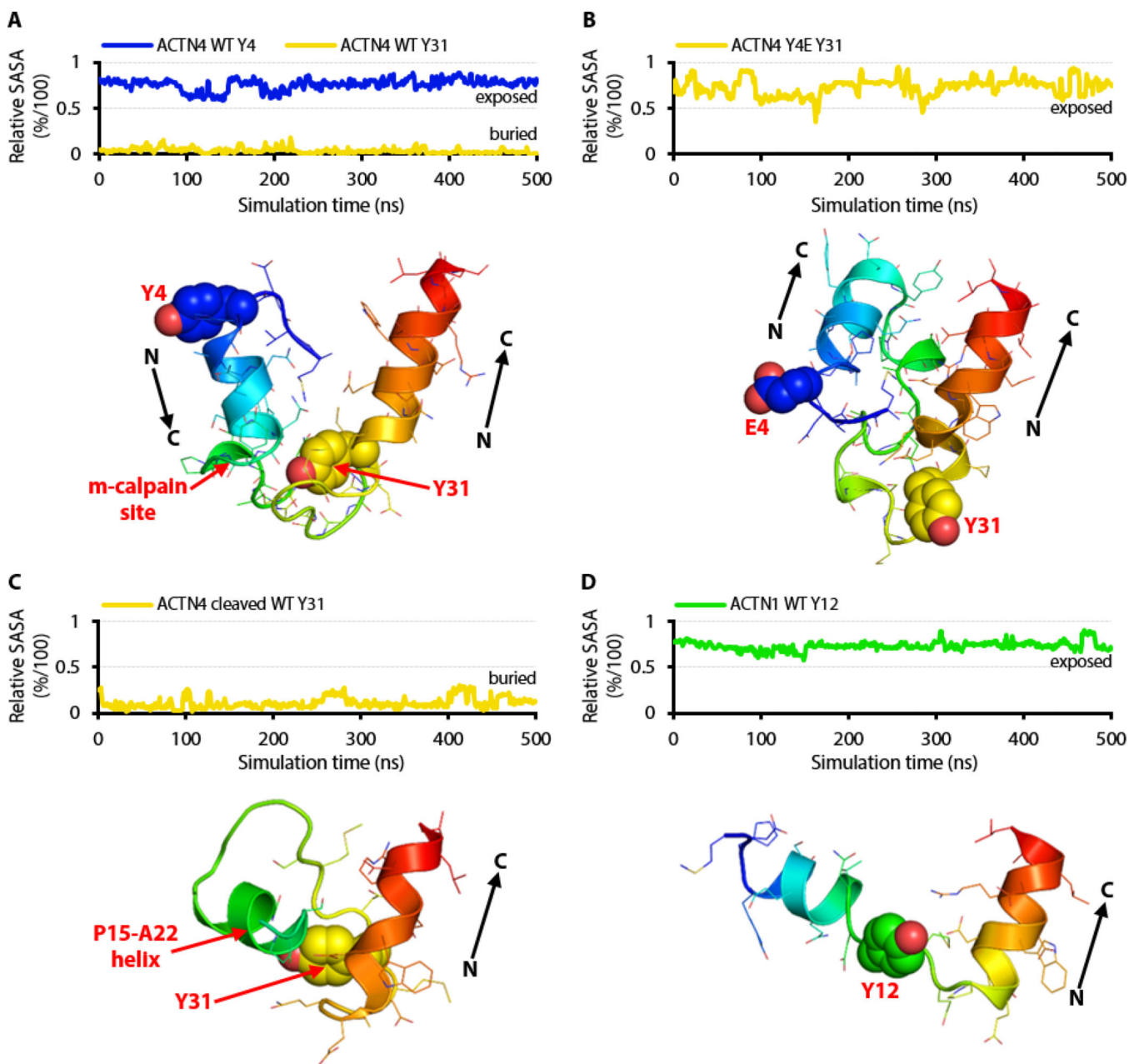
Figure 2. MDS predict that ACTN4 Tyr[31] is kinase inaccessible without phosphorylated Tyr[4]

Three independent MDS were performed for N-terminal constructs of wild-type ACTN4, Y4E ACTN4, truncated ACTN4, and wild-type ACTN1. In each panel, a representative relative solvent-accessible surface area (SASA) plot (top) and structure snapshot (bottom) are shown. Snapshots are displayed with rainbow coloring from dark blue to red in the N-to-C direction. (**A**) Tyr[4] and Tyr[31] (dark blue and yellow spheres) were mostly solvent exposed and buried (relative SASA: 71 ± 9% and 11 ± 8%), respectively. Two helices adopted an antiparallel arrangement that buried Tyr[31]. The primary m-calpain cleavage site (Tyr[13]-Gly[14] peptide bond; red arrow) was exposed. (**B**) Tyr[31] is mostly solvent exposed (relative SASA: 64 ± 13%) because the additional negative charge flipped the helices into a parallel

arrangement. (**C**) Removal of residues 1 to 13 led to a mostly helical region between Pro[15] to Ala[22] and kept Tyr[31] buried (relative SASA: 17 ± 8%). (**D**) ACTN1 was more extended due to its hydrophilic sequence, and Tyr[12] (green spheres) was mostly solvent exposed (relative SASA: 73 ± 12%). Relative SASA values are given as mean ± SD over the three MDS runs.
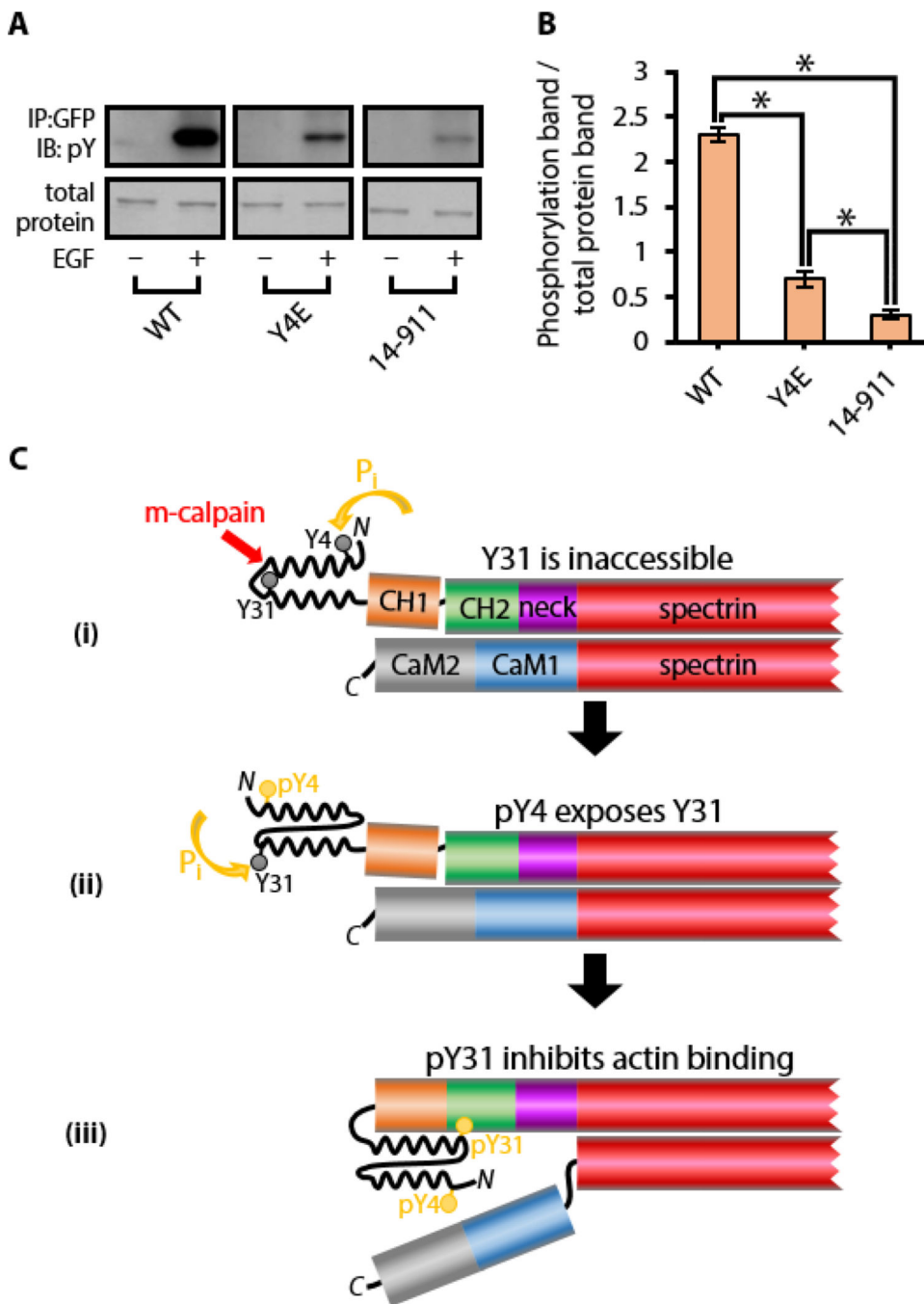
Figure 3. Tyr[31] phosphorylation in ACTN4 requires prior phosphorylation at Tyr[4]
(**A**) Representative gel of phosphorylation detection assay for wild-type (WT), Y4E, and 14-911 ACTN4-GFP constructs in the presence (+) or absence (−) of EGF. IP:GFP, immunoprecipitation with an antibody recognizing GFP; IB:pY, immunoblot with an antibody recognizing phosphorylated tyrosines. Total ACTN4-eGFP was detected with Coomassie blue G-250. (**B**) Quantitation of three experiments for the ratio of density units between phosphorylated tyrosine band over total protein band for each ACTN4 construct. Error bars indicate SEM. [* $P < 0.05$, two-sided Student's t-test.] (**C**) Tandem

phosphorylation model for the ACTN4 disordered N-terminal region. (i) Tyr^4 and Tyr^{31} are initially accessible and inaccessible, respectively, for phosphorylation (P_i), and Tyr^4 gets phosphorylated (pY4). (ii) Phosphorylation of Tyr^4 triggers structural changes in the disordered N-terminal region that lead to the exposure of Tyr^{31} and its phosphorylation (pY31). (iii) Phosphorylated Tyr^{31} inhibits binding of ACTN4 to actin by latching the two CH domains of the ABD in a closed configuration. Wavy lines in the N-terminal region denote alpha-helical structures. Red arrow indicates the m-calpain cleavage site between Tyr^{13}-Gly^{14}.
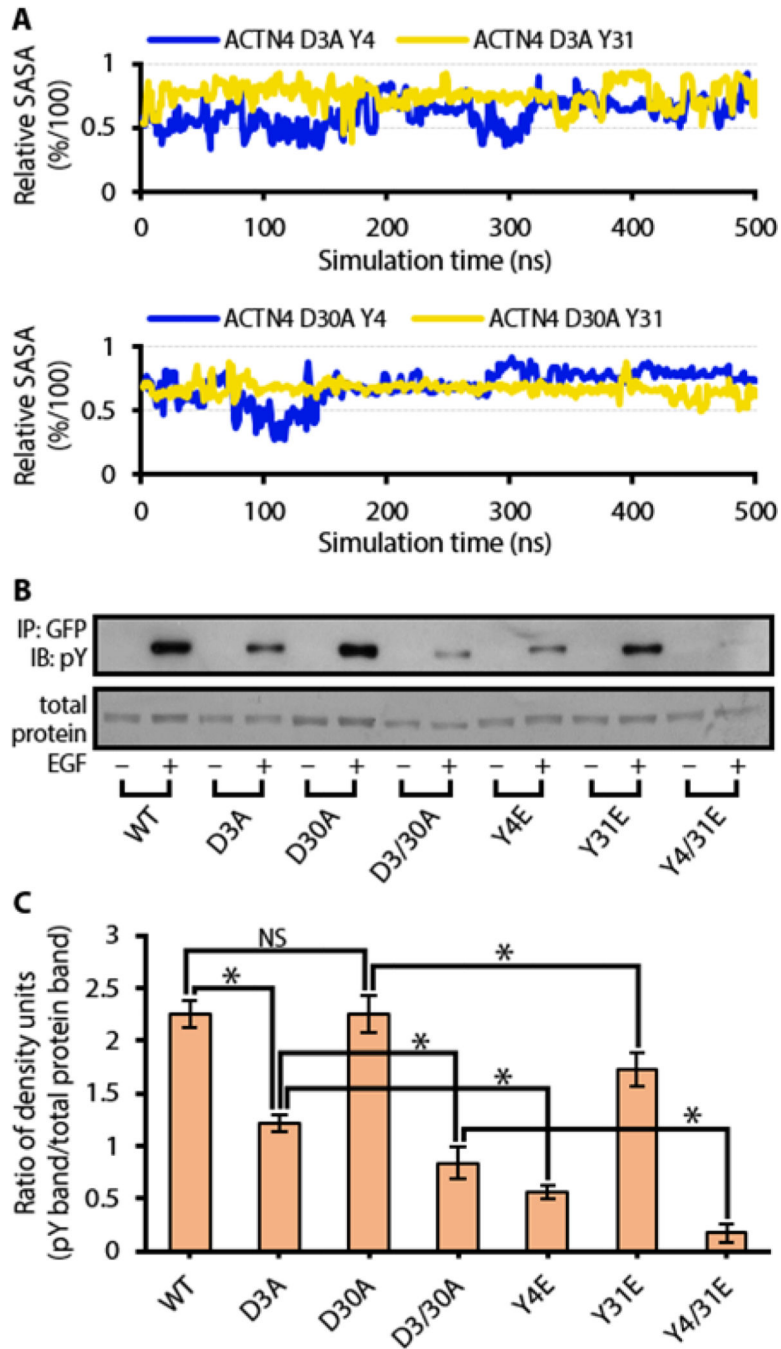
Figure 4. Phosphorylation of ACTN4 Tyr[4] is decreased upon mutation of the adjacent Asp[3]
(**A**) Representative plots (for one out of three independent MDS) showing relative SASA of Tyr[4] and Tyr[31] from D3A (top) and D30A (bottom) ACTN4 constructs. These mutations lead to both Tyr[4] and Tyr[31] being mostly solvent exposed (relative SASA of Tyr[4] and Tyr[31]: $67 \pm 14\%$ and $66 \pm 14\%$ for D3A, $66 \pm 12\%$ and $64 \pm 9\%$ for D30A). Relative SASA values are given as mean $\pm$ SD over the three runs. (**B**) Representative gel of phosphorylation detection assay for wild-type (WT), D3A, D30A, D3/30A, Y4E, Y31E, and Y4/31E ACTN4-GFP constructs in the presence (+) or absence (−) of EGF. IP:GFP,

immunoprecipitation with an antibody recognizing GFP; IB:pY, immunoblot with an antibody recognizing phosphorylated tyrosines. Total ACTN4-eGFP protein was detected with Coomassie blue G-250. (**C**) Quantitation of three experiments for the ratio of density units between phosphorylated tyrosine band over total protein band for each ACTN4 construct. Error bars indicate SEM. [* $P < 0.05$ based on two-sided Student's t-test. NS, not significant.]
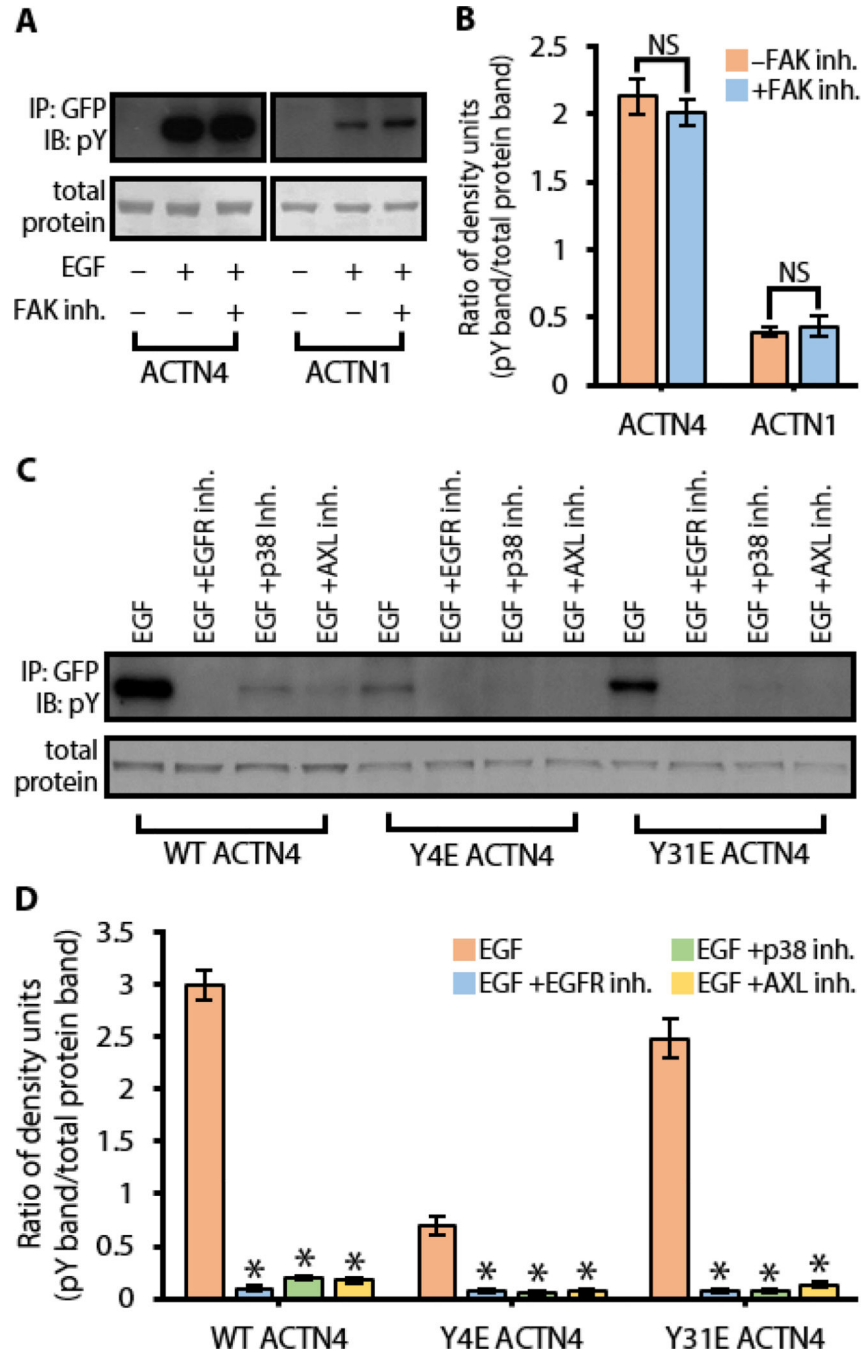
Figure 5. TAM family members, but not FAK, may be involved in EGF-induced phosphorylation of ACTN4

(**A**) Representative gel of EGF-induced phosphorylation detection assay for ACTN4-GFP and ACTN1-GFP in the presence (+) or absence (−) of 10 µM FAK inhibitor II. (**B**) Quantitation of three experiments for the ratio of density units between phosphorylated tyrosine band over total protein band for ACTN4 or ACTN1. Error bars indicate SEM. [NS, not significant.] (**C**) Representative gel of phosphorylation detection assay for wild-type (WT), Y4E, and Y31E ACTN4-GFP constructs in the presence of EGF alone or with one of the following: 10 µM EGFR inhibitor (PD153035), 15 µM p38 inhibitor (SB203580), or 15

μM TAM inhibitor (R428). (**D**) Quantitation of three experiments for the ratio of density units between phosphorylated tyrosine band over total protein band for each ACTN4 construct. Error bars indicate SEM. [* $P < 0.05$ based on two-sided Student's t-test.] IP:GFP, immunoprecipitation with an antibody recognizing GFP; IB:pY, immunoblot with an antibody recognizing phosphorylated tyrosines. Total ACTN4-eGFP protein was detected by staining with Coomassie blue G-250.
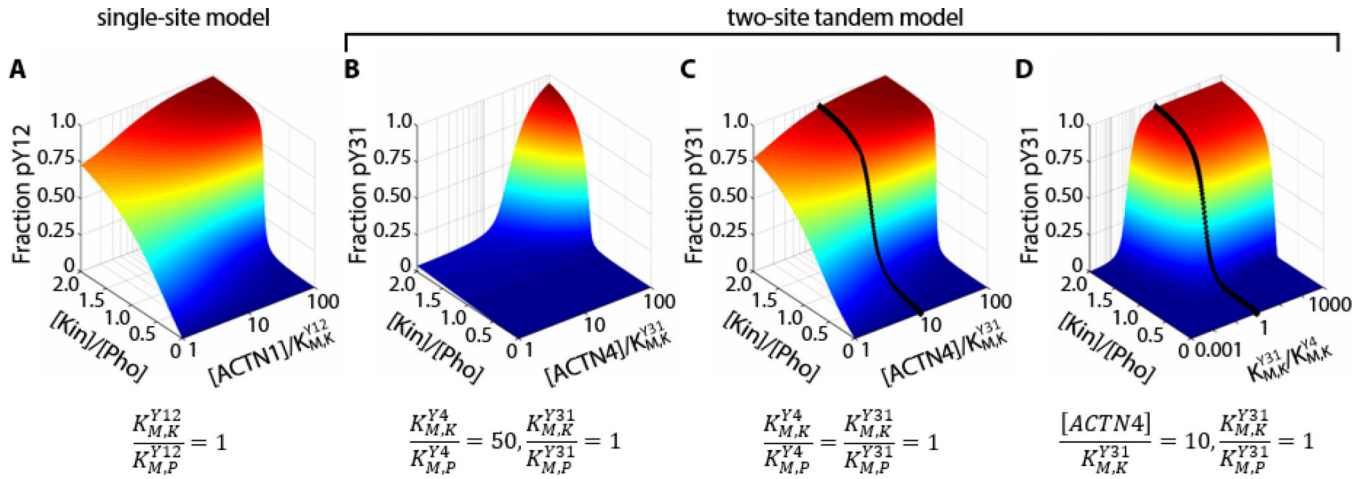
Figure 6. Tuning the kinase affinity of Tyr[4] is enough to design a switch
(**A**) Modeling results for phosphorylation in a single-site model (such as in ACTN1). Fraction of phosphorylated site is plotted against the ratio of kinase/phosphatase concentrations ([Kin]/[Pho]) and total ACTN1 concentration normalized by the kinase K_M ($[\text{ACTN1}]/K_{M,K}^{Y12}$; plotted as log scale). The K_M of the kinase and phosphatase for the site are set equal. (**B**) Results for phosphorylation of the functional site in a 1-kinase/1-phosphatase (1K1P) two-site tandem model (such as in ACTN4), where the kinase has a 50-fold weaker affinity for the switch site $(K_{M,K}^{Y4})$ than the functional site $(K_{M,K}^{Y31})$. Axes are similar as in (**A**). (**C**) Results for same model as in (**B**), but where the kinase has the same $K_{M,K}$ for both sites. Black curve shows the amount of phosphorylated Tyr[31] as a function of [Kin]/[Pho] when $[\text{ACTN4}]/K_{M,K}^{Y31}=10$. (**D**) Results for the 1K1P two-site tandem model where the fraction of phosphorylated site is plotted against [Kin]/[Pho] and the kinase K_M ratio for both sites $(K_{M,K}^{Y31}/K_{M,K}^{Y4})$, with $[\text{ACTN4}]/K_{M,K}^{Y31}=10$. Black curve shows the amount of phosphorylated Tyr[31] as a function of [Kin]/[Pho] when $K_{M,K}^{Y31}/K_{M,K}^{Y4}=1$. All enzyme concentrations are assumed to be directly proportional to their activities.